International Journal of Mass Spectrometry 438 (2019) 115–123

Contents lists available at ScienceDirect

International Journal of Mass Spectrometry

journal homepage: www.elsevier.com/locate/ijms

Correlation between the velocity scattering angle and product relative translational energy for S_N2 reactions. Comparison of experiments and direct dynamics simulations

Jing Xie[a], Jiaxu Zhang[b], Rui Sun[c], Roland Wester[d], William L. Hase[e,*]

[a] Department of Chemistry, University of Minnesota, Minneapolis, MN, 55455, USA
[b] MIIT Key Laboratory of Critical Materials Technology for New Energy Conversion and Storage, School of Chemistry and Chemical Engineering, Harbin Institute of Technology, Harbin, 150001, PR China
[c] Department of Chemistry, University of Hawaii, Manoa, Honolulu, HI, 96822, USA
[d] Institut für Ionenphysik und Angewandte Physik, Universität Innsbruck, Technikerstrasse 25, 6020, Innsbruck, Austria
[e] Department of Chemistry and Biochemistry, Texas Tech University, Lubbock, TX, 79401, USA

ARTICLE INFO

Article history:
Received 23 September 2018
Received in revised form
23 December 2018
Accepted 3 January 2019
Available online 10 January 2019

Keywords:
Direct dynamics simulations
Molecular beam, ion imaging experiments
SN2 reactions
Product translational energies
Velocity scattering angle

ABSTRACT

In previous research, direct dynamics simulations have been used to provide atomistic information for the $Cl^- + CH_3I$, $F^- + CH_3I$, and $OH^- + CH_3I$ S_N2 and proton transfer (PT) reactions. An important component of these simulations is comparison with molecular beam, ion imaging experiments. From the simulations, comparisons may be made with the product translational energy distributions determined from the experiments and the simulations give quite good agreement with these distributions. Though the experiments provide the in-plane angular distribution for a reaction's product translational energy distribution, the number of direct dynamics trajectories for a simulation is not sufficient to compare with this angular distribution. In the work presented here, the average percentage product translational energy partitioning for forward scattered events with scattering angle $\theta = 0–90^\circ$ and for backward scattered events with $\theta = 90–180^\circ$ are compared for the experiments and simulations. Overall good agreement is found, with a maximum difference as high as 5–10%. Additional atomistic details, regarding the dynamics of these reactions, are provided by scatter plots of their product relative translational energy versus the scattering angle θ.

1. Introduction

Crossed molecular beam ion-imaging experiments have provided detailed information regarding the dynamics of gas-phase S_N2 nucleophilic substitution reactions [1–10]. The experiments measured the angular distribution of the scattered products, with respect to the reactants relative velocity, and also the translational energy distribution of the reaction products at each scattering angle. The S_N2 reactions studied are those for $Cl^- + CH_3I$ [1,2], $F^- + CH_3I$ [3–6], and $OH^- + CH_3I$ [7–9]. For $OH^- + CH_3I$ and $F^- + CH_3I$, the proton transfer pathways to form $H_2O + CH_2I^-$ and $HF + CH_2I^-$ were also studied [9,11].

Direct chemical dynamics simulations have been performed to provide an atomic-level interpretation of the experimental measurements [1–5,7,9,10]. The simulations are in overall quite good agreement with the experimental measurements. The average energy partitioned to product relative translation, versus reactant collision energy, agrees with experiment for each of the reactions. In addition, the experimental and simulation product angular distributions are similar, and the simulations give an atomistic and mechanistic understanding of the origin(s) of the angular scattering. In addition to these direct dynamics simulations, simulations have also been performed using analytic potential energy functions and the results compared with experiment [12,6,13–15].

The previous comparisons between experiment and the direct dynamics simulations did not compare the correlation between the velocity scattering angle and the product relative translational energy as measured in the experiments. This is because an insufficient number of direct dynamics trajectories were calculated to prepare ion images versus scattering angle and product relative translational energy as determined in the experiments. However, a less refined comparison is possible by preparing scatter plots of the product translational energy, versus scattering angle, as obtained from the simulations. These plots are presented here for the Cl^- +

* Corresponding author.
E-mail address: bill.hase@ttu.edu (W.L. Hase).

https://doi.org/10.1016/j.ijms.2019.01.003
1387-3806/

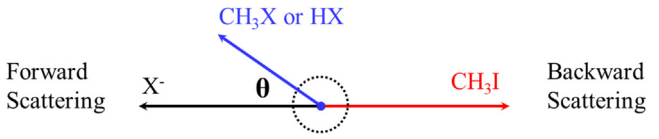

Scheme 1. An illustration of velocity scattering angle θ for X^- + CH_3I S_N2 or PT pathways. X = Cl, F, OH.

CH_3I, F^- + CH_3I, and OH^- + CH_3I direct dynamics simulations. Also presented from the simulations are the average percentages of the available product energy partitioned to product relative translation for the 0–90° and 90°–180° scattering angles. These percentages are compared with the values obtained from the experiments. Other details of the direct dynamics simulations, and their results, have been presented and discussed previously [1–5,7,9,10].

2. Correlation between the velocity scattering angle and product relative translational energy, and comparison with experiment

The velocity scattering angle is defined so that for θ = 0° the velocity vector of CH_3X or HX product is pointing in the same direction as that of reactant X^- for the S_N2 or PT reactions; i.e. see Scheme 1.

Before considering the correlation between the velocity scattering angle and the product relative translational energy it is meaningful to review the atomic-level mechanisms found for the reactions from previous simulations [1–5,7,9,10]. The results are summarized in Table 1. There are three direct mechanisms, rebound, stripping, and front-side attack. Indirect mechanisms are pre- and/or post-reaction complex formation, the roundabout, barrier recrossing(s), and combinations of these mechanisms. The complexes include ion-dipole and hydrogen-bonded S_N2 complexes and a proton transfer complex. For the OH^- + CH_3I reaction, the S_N2 and proton transfer pathways and complexes are coupled. The small number of barrier recrossing events are included with the complex percentage.

Angular distributions for product energy transfers of the different reactions are discussed in the following. Scatter plots of the product relative translational energy E'_{rel} versus scattering angle, obtained from the simulations, are given in Figs. 1–3. The probability of collision at a specific impact parameter b is proportional to b and the area of the points in the scatter plots are proportional to the value of b for the trajectory. To better distinguish the points, the color was varied from red to yellow as b increases. Average percentages of the available product energy released to relative translation are given in Table 2 for the 0–90° and 90°–180° ranges of the scattering angle θ. The former is for forward and the latter for backward scattering. Uncertainties in the average product relative translational energies for forward and backward scattering were not determined for the experiments, but were determined for the total the scattering. The percentage uncertainty in this energy for the total scattering ranges from 11 to 17% for F^- + CH_3I and 4–6% for OH^- + CH_3I [4,9]. The average product relative translational energy versus these scattering angle ranges is given in Table S1 of the Supporting information for the different reactions.

2.1. Cl^- + CH_3I S_N2 reaction

As shown in Table 2, for the Cl^- + $CH_3I \rightarrow ClCH_3 + I^-$ simulations [2] the percentage energy transfer to product relative translation (E'_{rel}) is higher for the backward scattered events with θ of 90–180° than for the forward scattered events. This is most pronounced for the simulations with a collision energy of 1.07 eV. This is consistent with the rebound mechanism, with backward scattering, which releases more energy into E'_{rel} than for the stripping mechanism with forward scattering. For the 0.20 eV simulations, if statistical uncertainties are considered, the percentage energy transfer to E'_{rel} is the same for backward and forward scattered events. This is a result of the importance of complex formation for this collision energy, which leads to isotropic scattering.

Table 1
Atomic-Level Mechanisms versus Reactant Relative Translational Energy for the Cl^- + CH_3I, F^- + CH_3I, and OH^- + CH_3I Reactions.

E_{rel}(eV)	Reaction Mechanisms and Percentages			
Cl^- + $CH_3I \rightarrow ClCH_3 + I^-$, MP2				
1.9	Rebound (73)	Stripping (9)	Roundabout (18)	
1.07	Rebound (100)			
0.76	Rebound (87)	Roundabout (8)	Complex (5)	
0.39	Rebound (88)	Stripping (11)	Complex (1)	
0.20	Rebound (17)	Complex (83)		
Cl^- + $CH_3I \rightarrow ClCH_3 + I^-$, DFT/BhandH				
0.39	Rebound (82)	Stripping (6)	Complex (12)	
0.20	Rebound (30)	Complex (70)		
F^- + $CH_3I \rightarrow FCH_3 + I^-$, DFT/B97-1				
1.53	Rebound (29)	Stripping (12)	Complex (59)	
0.32	Rebound (15)	Stripping (25)	Complex (60)	
F^- + $CH_3I \rightarrow FCH_3 + I^-$, MP2				
1.53	Rebound (46)	Stripping (43)	Complex (11)	
F^- + $CH_3I \rightarrow HF + CH_2I^-$, DFT/B97-1				
1.53	Rebound (10)	Stripping (57)	Complex (33)	
OH^- + $CH_3I \rightarrow CH_3OH + I^-$, DFT/B97-1				
2.0	Rebound (30)	Stripping (64)	Front-side (3)	Roundabout (3)
1.0	Rebound (18)	Stripping (63)	Roundabout (5)	Complex (14)
0.5	Rebound (22)	Stripping (36)	Roundabout (4)	Complex (38)
0.05	Rebound (32)	Stripping (29)	Roundabout (1)	Complex (38)
OH^- + $CH_3I \rightarrow H_2O + CH_2I^-$, DFT/B97-1				
2.0	Rebound (13)	Stripping (87)		
1.0	Rebound (10)	Stripping (77)	Roundabout (10)	Complex (3)
0.5	Rebound (12)	Stripping (54)	Roundabout (6)	Complex (28)
0.05	Rebound (12)	Stripping (32)	Complex (56)	

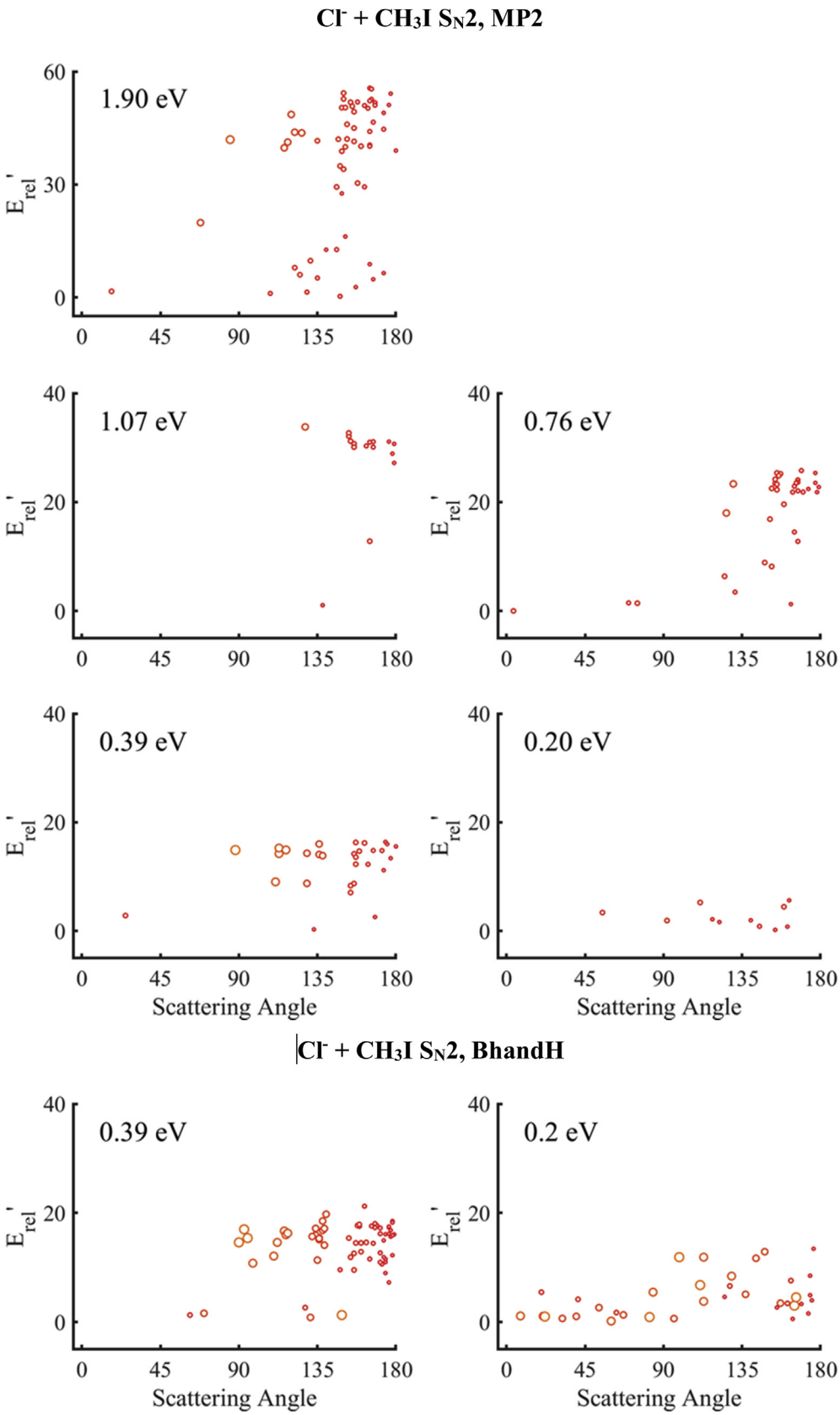

Fig. 1. Scatter plots of energy transfer to product relative translational energy E'_{rel} (kcal/mol) versus the scattering angle θ for the $Cl^- + CH_3I$ S_N2 reaction for MP2 and BhandH direct dynamics simulations. The probability of collision at a specific impact parameter b is proportional to b and the area of the points in the scatter plots are proportional to the value of b for the trajectory. To better distinguish the points, the color was varied from red to yellow as the impact parameter increases.

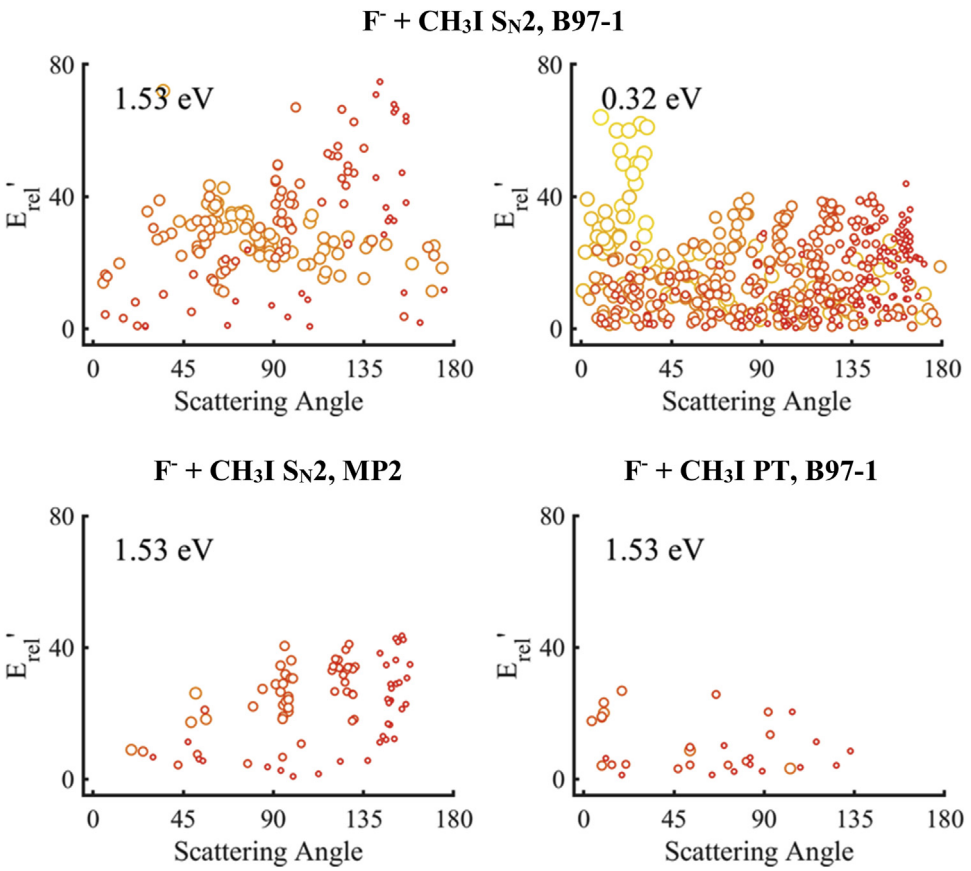

Fig. 2. Same as Fig. 1, but for the F^- + CH_3I S_N2 and proton transfer (PT) direct dynamics simulations with B97-1 and F^- + CH_3I S_N2 with MP2.

As shown in Fig. 1, for the MP2 simulations there are very few scattering events for $\theta = 0–90^\circ$ and comparison with experiment is uncertain for these scattering angles. This results in part from sampling of the impact parameter b for the simulations. The low reaction probability at large b makes it computationally intractable to sample the complete range of b, which has the effect of suppressing forward scattering that is important for large b. However, for $\theta = 90–180^\circ$ there are more simulation scattering events and statistically meaningful comparisons may be made between simulation and experiment. There is good agreement for E_{rel} of 0.76, 1.07, and 1.9 eV, but not for 0.39 eV. For this E_{rel}, the experimental scattering is isotropic, e.g. the same percentage average energy transfer for both θ of 0–90°and 90–180°, and the $P(E'_{rel})$ distribution is in agreement with phase space theory (PST), suggesting that the reaction is indirect and proceeds through S_N2 complexes. In contrast, for the MP2 simulations at 0.39 eV 99% of the reaction is direct, dominated by the rebound mechanism with backward scattering, and the average E'_{rel} is much higher than found experimentally. However, for the simulations at E_{rel} = 0.20 eV, the dynamics are similar to those for the experiments at 0.39 eV; i.e., 83% of the reaction is indirect and the experimental and simulation average E'_{rel} agree. As discussed below, there was some uncertainty in E_{rel} for the experiments identified as performed at E_{rel} = 0.39 eV and the actual E_{rel} is lower, reducing the extent of disagreement between experiment and simulation.

There is qualitative agreement between the MP2 and BhandH simulations for E_{rel} = 0.39 and 0.20 eV, but not quantitative. Both theories predict that the Cl^- + CH_3I S_N2 reaction is predominately direct at 0.39 eV and indirect at 0.20 eV, but their detailed atomistic dynamics are different. For MP2 99% of the reaction is direct at 0.39 eV, while 88% for BhandH. At 0.20 eV 17% of the reaction is direct with MP2, but 30% with BhandH. At 0.39 eV the energy partitioning to energy $E'_{rel}$is statistically the same for MP2 and BhandH, but at 0.20 eV BhandH partitions significantly more to E'_{rel}.

There is considerable interest in comparing direct dynamics atomistic mechanisms for different electronic structure theories [2,16]. MP2 and BhandH have the same direct rebound (DR) and stripping (DS) mechanisms, and their relative probabilities are similar for the two theories. At 0.39 eV the DR/DS ratio is 8 for MP2 and 14 for BhandH, and given statistical uncertainties these ratios are quite similar. At 0.20 eV the only direct mechanism is DR for both MP2 and BhandH. The relative importance of the multiple indirect mechanisms are quite different for MP2 and BhandH. At 0.39 eV, formation of both the Cl^--–CH_3I (A) and $ClCH_3$–I^- (B) pre- and post-reaction complexes is the only MP2 indirect mechanism. However, for BhandH there are four indirect mechanisms, with only formation of A dominant and formation of both A and B, the roundabout (Ra) + A, and Ra + B less important. At 0.20 eV, A + B + barrier recrossing (br) is dominant for MP2, with Ra + A not as important. The indirect dynamics are much different for BhandH at 0.20 eV. Formation of A is dominant, with A + B almost as important and a small contribution from Ra + A.

2.2. F^- + CH_3I S_N2 reaction

As shown in Table 2, the angular dependence of the product energy partitioning for the F^- + CH_3I S_N2 reaction is similar for the experiments and the B97-1 simulations [3,4]. There is a complete sampling of the impact parameter in these simulations, and direct comparisons with experiment may be made for E_{rel} of 1.53 and 0.32 eV. For the backward scattered events, $\theta = 90–180^\circ$, the energy

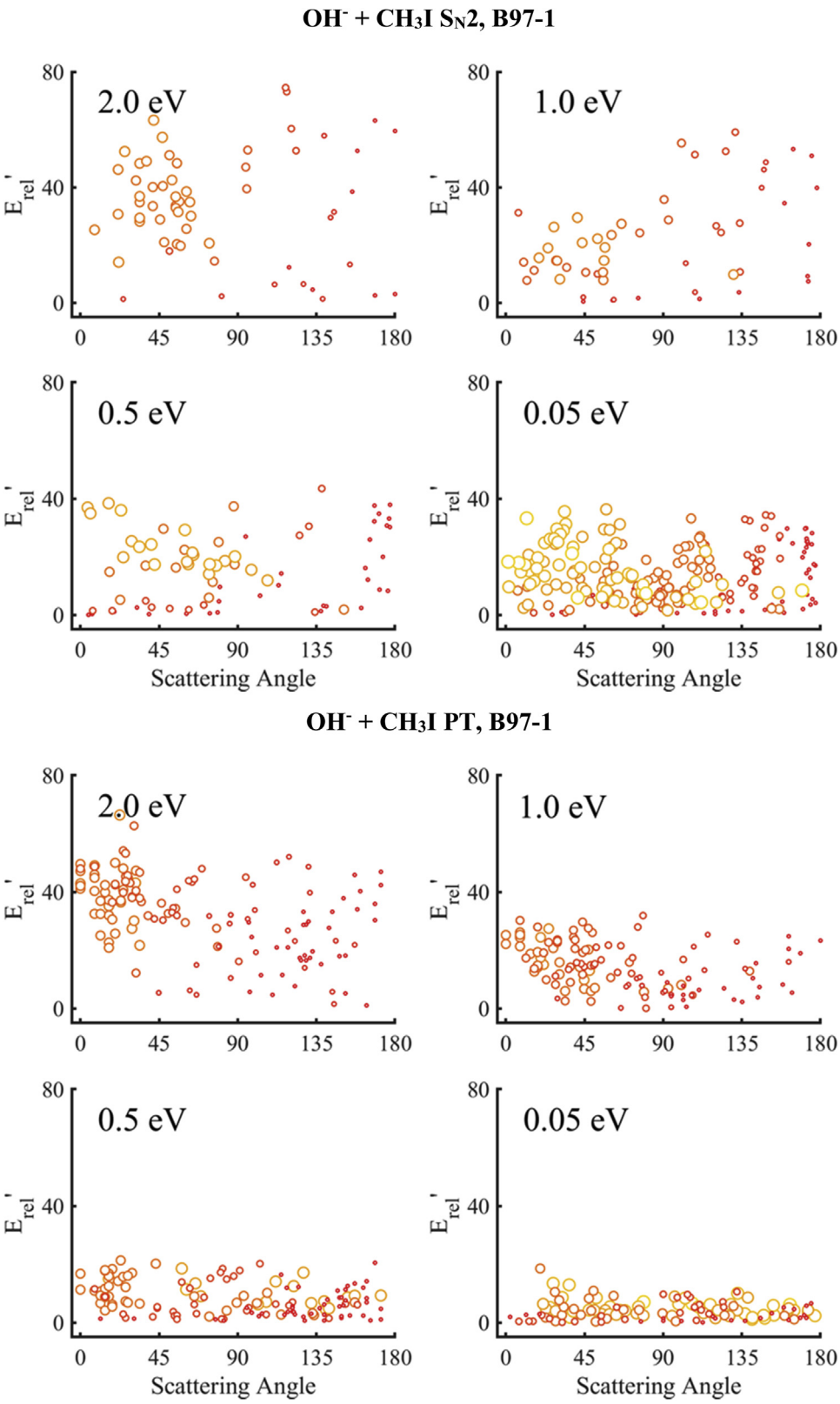

Fig. 3. Same as Fig. 1, but for the OH^- + CH_3I S_N2 and proton transfer (PT) direct dynamics simulations with B97-1.

partitioning to E'_{rel} is somewhat lower in the simulations, but not significantly. The experiments show that more energy is transferred to E'_{rel} for backward scattering. The scatter plots of energy transfer to E'_{rel} versus θ in Fig. 2 indicate that at low E_{rel} of 0.32 eV there are events at small θ which transfer a large percentage to E'_{rel}, while at high E_{rel} of 1.53 eV large transfer to E'_{rel} occurs for large θ. The latter large transfer to E'_{rel}, for large θ, is consistent with the rebound mechanism.

MP2 direct dynamics were also used to study the F^- + CH_3I S_N2 reaction at E_{rel} = 1.53 eV [5]. The MP2 potential energy surface

Table 2
Average Percentage of Product Relative Translational Energy versus Scattering Angle for $Cl^- + CH_3I$, $F^- + CH_3I$, and $OH^- + CH_3I$ Reactions[a].

	Angle: 0 – 90°		Angle: 90 – 180°	
E_{rel}(eV)	Exp	Sim	Exp	Sim
$Cl^- + CH_3I$ (S_N2), MP2				
1.9	43%	49% ± 15%	67%	67% ± 4%
1.07	42%		75%	70% ± 5%
0.76	40%	[b]	69%	58% ± 4%
0.39	28%	47% ± 14% 28%		49% ± 3%
0.2		17% ± 1%		12% ± 3%
$Cl^- + CH_3I$ (S_N2), BhandH				
0.39	28%	43% ± 16%	28%	52% ± 2%
0.2		8% ± 2%		30% ± 3%
$F^- + CH_3I$ (S_N2), B97-1				
2.34	31%		47%	
1.81	33%		49%	
1.53	34%	32% ± 1%	51%	42% ± 2%
0.69	32%		39%	
0.32	30%	31% ± 1%	40%	31% ± 1%
	$F^- + CH_3I$ (S_N2), MP2			
1.53	34%	25% ± 2%	51 %	35% ± 1%
$F^- + CH_3I$ (proton transfer), B97-1				
1.53		32% ± 4%		26% ± 6%
$OH^- + CH_3I$ (S_N2), B97-1				
2	23%	29% ± 2%	30%	43% ± 5%
1.5	26%		34%	
1.0	26%	22% ± 2%	31%	35% ± 4%
0.5	31%	26% ± 2%	35%	20% ± 3%
0.05		24% ± 1%		22% ± 1%
$OH^- + CH_3I$ (proton transfer), B97-1				
2.0		72% ± 3%		56% ± 3%
1.0		57% ± 4%		33% ± 5%
0.5		59% ± 6%		37% ± 3%
0.05		41% ± 8%		36% ± 6%

[a] The uncertainties in the simulation percentages are standard deviations. Uncertainties in the experimental percentages are discussed in the third paragraph of Section 2.
[b] There were not a sufficient number of simulation data points to have an accurate analysis.

in the entrance channel for the $F^- + CH_3I$ S_N2 reaction has both the traditional ion-dipole C_{3v} potential energy minimum as well as a hydrogen-bonded minimum, whereas B97-1 has only the latter [16]. The MP2 and B97-1 simulations are in overall good agreement with respect to product energy partitioning at E_{rel} = 1.53 eV. The average fraction of the available product energy partitioned to CH_3F rotation and vibration is 0.66 ± 0.1 and 0.63 ± 0.04 for MP2 and B97-1, respectively. The experimental fraction is 0.59 ± 0.08. In comparing the MP2 and B97-1 velocity scattering angle distributions at E_{rel} = 1.53 eV, the MP2 distribution is in better agreement with experiment. The MP2 scatter plot of energy transfer to E'_{rel} versus θ is given in Fig. 2, where it may be compared with the B97-1 scatter plot. Overall the scatter plots are similar, but B97-1 has some translational energies near 80 kcal/mol, while for MP2 all the energies are less than 40 kcal/mol. This results in a slightly higher average E'_{rel} for B97-1.

2.3. $F^- + CH_3I$ PT reaction

For E_{rel} = 1.53 eV $F^- + CH_3I \rightarrow HF + CH_2I^-$ proton transfer occurs and this reaction was studied with B97-1 simulations [17]. The scatter plot of the products' relative translational energy versus scattering angle is given in Fig. 2. The scattering angle extends to ~130° and the product energy transfer distribution is not strongly dependent on scattering angle. As shown in Table 2, this results in similar product energy partitioning for the forward scattering, θ = 0–90°, and the backward scattering, θ = 90–180°.

2.4. $OH^- + CH_3I$ S_N2 reaction

For the B97-1 simulations of the $OH^- + CH_3I$ S_N2 reaction there was complete sampling of the impact parameter [9]. As shown in Table 2, the angular dependence of the energy partitioning to E'_{rel} found from the simulations is in semi-quantitative agreement with experiment, with differences only as large as 15%. The experiments give a slightly higher percentage energy transfer to E'_{rel} for the backward scattered events with θ of 90–180°. This is seen in the simulations for the collision energies of 2.0 and 1.0 eV. At 0.5 eV, the experimental forward scattering percentage energy transfer to E'_{rel} is higher by 4% than that for backward scattering. In comparison, the simulations predict energy transfer to be 6% lower for forward than for backward scattering. Experimentally, the difference in the E'_{rel} percentage between forward and backward scattering decreases from 13% to 8%, 5%, and 4% as the collision energy decreases from 2.0 eV to 1.5, 1.0, and 0.5 eV, respectively. It is anticipated that as the collision energy keeps decreasing, the E'_{rel} percentage will become similar for the forward and backward scattering, partly due to the dominance of indirect mechanisms. This similarity is reflected at 0.05 eV, where the E'_{rel} percentage is 24% for forward scattering and 22% for backward scattering.

As shown by the scatter plots in Fig. 3 of E'_{rel} versus θ, large energy transfer to E'_{rel} is only important for the high collision energies of 1.0 and 2.0 eV. For the lower collision energies of 0.05 and 0.5 eV, energy transfer to E'_{rel} has a maximum of only ~40 kcal/mol. The scatter plots in Fig. 3 shows that the simulation scattering is strongly forward, i.e. θ = 0–90°, at collision energies of 2.0 and 1.0 eV, and the scattering becomes more isotropic at the lower col-

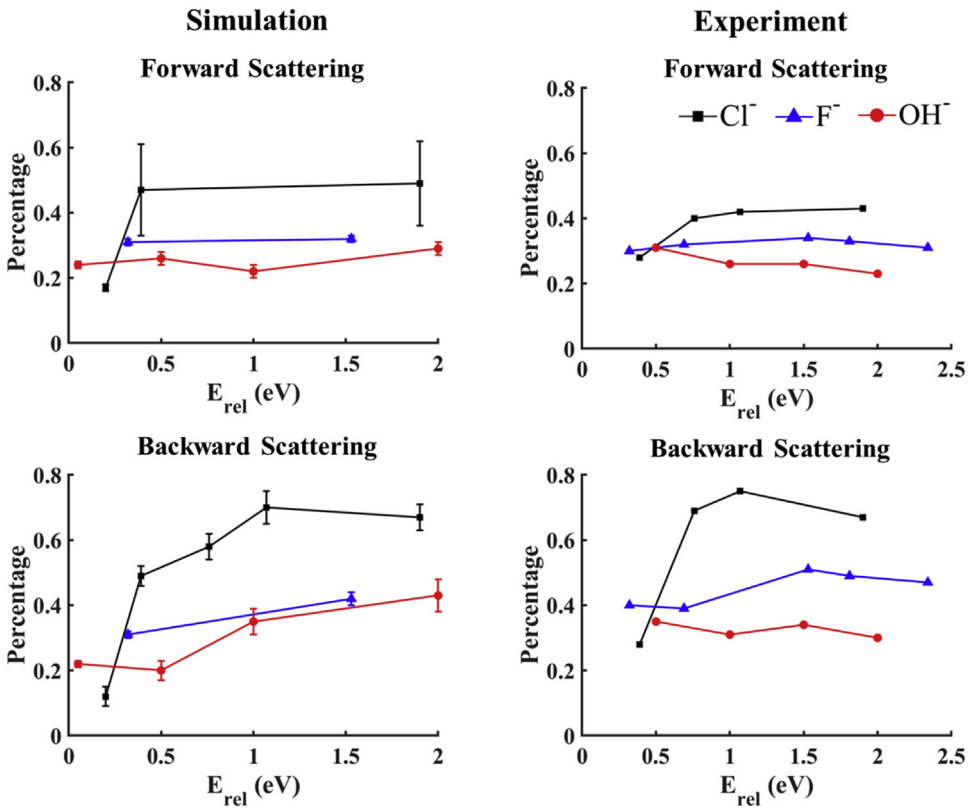

Fig. 4. Plot of the percentage of energy transfer to product relative translational energy E'_{rel} versus collision energy E_{rel} (in eV) for the S_N2 reactions of Cl^- +CH_3I, black square —■—; F^- + CH_3I, blue triangle —▲—; OH^- + CH_3I, red circle —●—. The level of theory is MP2, B97-1, and B97-1 for the three reactions, respectively. Results from simulations are on the left and from experiment on the right.

lision energies of 0.5 and 0.05 eV. However, experimentally, the isotropic scattering is observed for collision energies of 0.5, 1.0, 1.5, and 2.0 eV.

2.5. OH^- + CH_3I PT reaction

The OH^- + CH_3I → H_2O + CH_2I^- proton transfer reaction is exothermic and was studied for collisions with E_{rel} of 0.05, 0.5, 1.0, and 2.0 eV using B97-1 direct dynamics simulations [9]. The resulting scatter plots of product relative translational energy versus scattering angle are given in Fig. 3. At E_{rel} of 1.0 and 2.0 eV, the scattering is strongly forward, i.e. θ = 0–90°, in excellent agreement with experiments. However, for the other two E_{rel} the scattering is more isotropic. As shown in Table 2, for the lowest E_{rel} of 0.05 eV the average product energy partitioning is statistically the same for forward and backward scattering. For the other three E_{rel}, energy partitioning to product relative translation is larger for forward scattering.

3. Comparisons of product energy partitioning for the different reactions

It is of interest to compare differences in the product energy partitioning percentages, for the reactions of Cl^-, F^-, and OH^- with CH_3I. These comparisons are given in Fig. 4 for both S_N2 forward and backward scattering, and for both the simulation and experimental results. The striking result for backward scattering are the larger E'_{rel} percentages for the Cl^- + CH_3I S_N2 reaction than for the other reactions. For each reaction there is a decrease in percentage transfer to E'_{rel} with decrease E_{rel}. Though there are large uncertainties in the forward scattering percentage transfers to E'_{rel} for the Cl^- + CH_3I S_N2 reaction, they appear to be larger than the percentages for forward scattering of the other S_N2 reactions. For the lowest E_{rel} = 0.20 eV for the Cl^- + CH_3Cl S_N2 reaction, the E'_{rel} percentage from the MP2 simulations is 17 ± 2% for forward scattering and 12 ± 3% for backward scattering, similar to the 16% expected from PST [1,2]. For both forward and backward scattering, the percentages transferred to E'_{rel} are similar for the F^- + CH_3I and OH^- + CH_3I S_N2 reactions. The percentages are relatively independent of E_{rel} except for OH^- + CH_3I backward scattering.

For OH^- + CH_3I, the percentage energy transfer to E'_{rel} is higher for proton transfer than S_N2 reaction, particularly for forward scattering, as shown in Fig. 5. For both forward and backward scattering of OH^- + CH_3I proton transfer, the percentage transfer to E'_{rel} is highest for the largest E_{rel} of 2.0 eV and then decreases. For F^- + CH_3I proton transfer at the only E_{rel} = 1.53 eV, the percentage energy transfer to E'_{rel} for forward scattering is similar to that found for the F^- + CH_3I S_N2 reaction, but substantially lower for backward scattering. For forward scattering, the percentage transfer to E'_{rel} is much smaller for F^- + CH_3I than OH^- + CH_3I proton transfer.

As shown in Fig. 4, energy transfer to product translation is more important for the Cl^- S_N2 reaction than for the F^- and OH^- S_N2 reactions. As shown in Table 1, this result is consistent with more indirect reaction for F^- and OH^- than for Cl^-. Indirect mechanisms, including the roundabout,1 transfer less energy to product translation than do the direct rebound and stripping mechanisms [2–4,9]. At this time there is not a certain explanation to why energy transfer to product translation is smaller for OH^- than F^-.

For the OH^- + CH_3I reaction there is more energy transfer to product translation for proton transfer (PT) than for S_N2; see Fig. 5 [9]. For PT the fraction of the available energy transferred to product translation, varies from 0.71 to 0.38 for the highest to lowest collision energy E_{rel}. For S_N2 this fraction varies from 0.32 to 0.20.

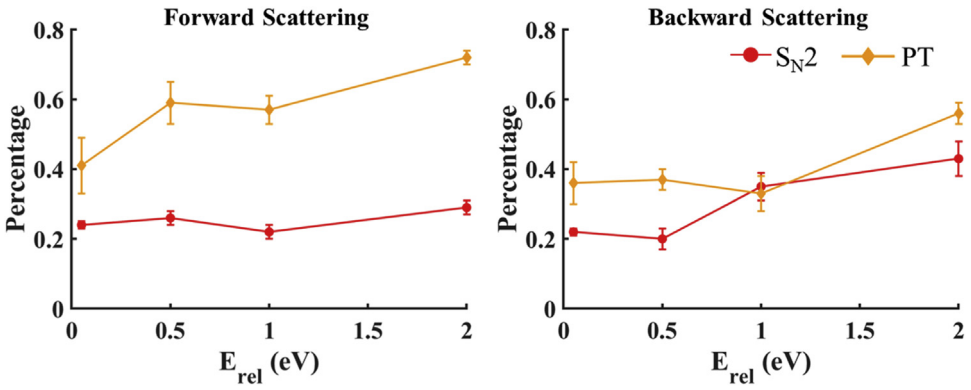

Fig. 5. Plot of the percentage of energy transfer to product relative translational energy E'_{rel} versus collision energy E_{rel} (in eV) for OH^- + CH_3I S_N2, red circle ; and PT, yellow diamond , reactions. Results from B97-1 simulations.

The dominant energy transfer pathway for S_N2 is to CH_3OH vibration, with CH_3OH rotation receiving less than 20% of the product energy. For PT energy transfer to rotation is more important than to vibration for both the CH_2I^- and H_2O products. CH_2I^- rotation receives up to ~30% of the product energy. The enhanced transfer of energy to product translation, for PT as compared to S_N2, may result from more stripping and less complex formation for PT as shown in Table 1.

As discussed above for the OH^- + CH_3I reaction, and shown in Fig. 5, PT transfers substantially more energy to product translation than S_N2 for forward scattering. The origin of these dynamics are uncertain. Complex formation is more important for S_N2 than PT (Table 1) and this may be an accentuating factor for forward scattering, reducing energy transfer to product translation for S_N2. In future work it would be interesting to determine the percentages of the different reaction mechanisms for both forward and backward scattering, and the transfers to the different product energies for each mechanism. Previous studies [2–4,9] have shown that the direct rebound and stripping mechanisms are preferentially backward and forward scattering, respectively, and complex formation results in isotropic scattering. Scattering angle distributions have not been quantified for the rebound mechanism. An implication is that OH^- + CH_3I energy transfer may result in more transfer to product translation for PT stripping as compared to S_N2 stripping.

4. Summary

In previous work classical trajectory direct dynamics simulations were performed to study atomistic details of the Cl^- + CH_3I [1,2], F^- + CH_3I [3–6], and OH^- + CH_3I [7–9] S_N2 reactions, and the proton transfer pathways of these reactants to form H_2O + CH_2I^- and HF + CH_2I^- [9,11]. Rate constants and product energy and velocity scattering angle distributions were determined from the simulations. A property determined from the molecular beam, ion imaging experiments is the correlation between the relative translational energy of the products and the reaction's velocity scattering angle. This property was not considered in the previous direct dynamics simulations, but was analysed here from the results of the previous simulations. A detailed analysis of this correlation is not possible given the sample sizes for the direct dynamics simulations, but a "coarse" analysis is possible for which the average product relative translational energy is calculated for both forward scattering trajectories, with θ = 0–90°, and backward scattering trajectories, with θ = 90–180°. Such an analysis was made here and it was found the average product relative translational energy from the simulations and experiments are in good agreement for both the forward and backward scattering dynamics of the Cl^- + CH_3I, F^- + CH_3I, and OH^- + CH_3I S_N2 reactions. This is the principal understanding obtained from this study, illustrating the agreement between simulation and experiment. Additional information regarding the reaction's product relative translational energy distribution, versus scattering angle, were obtained from scatter plots of the relative translational energy versus scattering angle. These analyses also show overall good agreement between the simulations and experiments.

Analyses of the S_N2 and PT reaction dynamics made here for Cl^- + CH_3I, F^- + CH_3I, and OH^- + CH_3I suggest the importance of determining the percentages of the different atomistic mechanisms for both forward and backward scattering and the product energy transfer distributions for these mechanisms. Such studies are of interest for future research.

Acknowledgements

The research at Texas Tech University was supported by the Robert A. Welch Foundation under Grant No. D-0005. J. Zhang thanks the National Natural Science Foundation of China (No. 21573052) for support of his research. W. L. Hase wishes to acknowledge important discussions with Javier Aoiz and Luis Bañares.

Appendix A. Supplementary data

Supplementary material related to this article can be found, in the online version, at doi:https://doi.org/10.1016/j.ijms.2019.01.003.

References

[1] J. Mikosch, S. Trippel, C. Eichhorn, R. Otto, U. Lourderaj, J.X. Zhang, W.L. Hase, M. Weidemüller, R. Wester, Science 319 (2008) 183–186.
[2] J. Zhang, U. Lourderaj, R. Sun, J. Mikosch, R. Wester, W.L. Hase, J. Chem. Phys. 138 (2013) 114309.
[3] J. Zhang, J. Mikosch, S. Trippel, R. Otto, M. Weidemüller, R. Wester, W.L. Hase, J. Phys. Chem. Lett. 1 (2010) 2747–2752.
[4] J. Mikosch, J. Zhang, S. Trippel, C. Eichhorn, R. Otto, R. Sun, W.A. de Jong, M. Weidemüller, W.L. Hase, R. Wester, J. Am. Chem. Soc. 135 (2013) 4250–4259.
[5] R. Sun, C.J. Davida, J. Zhang, W.L. Hase, Phys. Chem. Chem. Phys. 17 (2015) 2589–2597.
[6] M. Stei, E. Carrascosa, M.A. Kainz, A.H. Kelkar, J. Meyer, I. Szabó, G. Czakó, R. Wester, Nat. Chem. 8 (2016) 151–156.
[7] R. Otto, J. Xie, J. Brox, S. Trippel, M. Stei, T. Best, M.R. Siebert, W.L. Hase, R. Wester, Faraday Discuss. 157 (2012) 41–57.
[8] R. Otto, J. Brox, S. Trippel, M. Stei, T. Best, R. Wester, Nat. Chem. 4 (2012) 534–538.
[9] J. Xie, R. Sun, M.R. Siebert, R. Otto, R. Wester, W.L. Hase, J. Phys. Chem. A 117 (2013) 7162–7178.
[10] J. Xie, R. Otto, J. Mikosch, J. Zhang, R. Wester, W.L. Hase, Acc. Chem. Res. 47 (2014) 2960–2969.

[11] E. Carrascosa, T. Michaelsen, M. Stei, B. Bastian, J. Meyer, J. Mikosch, R. Wester, J. Phys. Chem. A 120 (2016) 4711–4719.
[12] I. Szabó, A.G. Császár, G. Czakó, Chem. Sci. 4 (2013) 4362–4370.
[13] I. Szabó, G. Czakó, J. Phys. Chem. A 121 (2017) 9005–9019.
[14] I. Szabó, B. Olasz, G. Czakó, J. Phys. Chem. Lett. 8 (2017) 2917–2923.
[15] I. Szabó, G. Czakó, J. Phys. Chem. A 121 (2017) 5748–5757.
[16] R. Sun, J. Xie, J. Zhang, W.L. Hase, Int. J. Mass Spectrom. 377 (2015) 222–227.
[17] J. Zhang, J. Xie, W.L. Hase, J. Phys. Chem. A 119 (2015) 12517–12525.